Limits on phonon information extracted from neutron pair-density functions

Matthias J. Graf, Il-Kyoung Jeong, Daniel L. Starr, R. H. Heffner
Los Alamos National Laboratory, Los Alamos, New Mexico 87545
(Dated: December 25, 2021)

We explore the possibility of extracting information about lattice dynamics in simple crystal structures from the neutron pair-density function (PDF) through inverse data analysis. Contrary to the claims by Dimitrov, Louca, and Röder [Phys. Rev. B **60**, 6204 (1999)], and in agreement with recent work by Reichardt and Pintschovius [Phys. Rev. B **63**, 174302 (2001)], we find that the PDF alone is not sufficient for constructing accurate phonon dispersions in the entire Brillouin zone in systems with complex lattice dynamics. However, our numerical simulations show that for monatomic *fcc* and *bcc* crystal structures it is, in principle, possible to obtain phonon moments of complex metals as well as phonon frequencies of simple metals within a few percent accuracy.

PACS numbers: 63.20.-e, 61.12.-q, 61.12.Bt
Keywords: lattice-dynamics, phonon-dispersion, neutron-diffraction, inverse-analysis

arXiv:cond-mat/0209540v1 [cond-mat.mtrl-sci] 23 Sep 2002

I. INTRODUCTION

Our goal in this work is to determine whether it is possible to obtain high-quality information about the phonon dispersion and lattice dynamics over the entire Brillouin zone (BZ) without having to measure the phonon dispersion in single crystals. This is an important question for materials where no single crystals are available, or when performing measurements at high pressure and high temperature. This work was motivated by the claim of Dimitrov and co-workers[1] that it is possible to extract accurate phonon dispersions by properly modeling the phonon system and applying an inverse data analysis technique to the *measured* neutron pair-density function (PDF). In principle, the PDF contains all the lattice dynamical information, although most of it is lost after the integration over dynamical and directional degrees of freedom is performed. Very recently, Reichardt and Pintschovius[2] seriously questioned the results of Dimitrov *et al.*,[1] and concluded that the PDF is rather insensitive to the precise shape of the dispersion curves, and, therefore, that there is no hope for extracting lattice vibrations from experimental PDF measurements. Similar concerns were raised by Mellergård and McGreevy.[3]

Experimental PDF data obtained from neutron powder diffraction require various corrections to the raw data, which introduce additional errors in the analysis. Thus, in this paper we studied *synthetic* data sets to avoid any ambiguity in the analysis. We tested and utilized standard reverse Monte Carlo[4] and Levenberg-Marquardt[5] methods for the inverse analysis of the PDF spectra to determine how much lattice dynamical information can be recovered. To do that, we generated synthetic PDF data sets for various monatomic *fcc* and *bcc* crystal structures from published tables of generalized Born-von Kármán (BvK) force constants.[6] We used a BvK model to describe the lattice dynamics since it is easy to implement and is well documented in the literature, although it is not the best-suited phonon model for metals. This gave us full control when testing the robustness and accuracy of the inverse analysis methods being used. We emphasize that we wished to determine whether a unique relationship exists between the phonon dispersion and the corresponding PDF of the system, *not* a unique relationship between the force constants of the phonon model and its dispersion or PDF spectrum.

Our study of the inverse (indirect) problem of extracting phonons from a given PDF spectrum complements the previous studies by Reichardt and Pintschovius,[2] who studied the forward (direct) problem of obtaining a unique PDF spectrum from very different phonon dispersion curves.

II. ANALYSIS

We calculated the PDF spectrum by Fourier transforming the powder-averaged, coherent static structure factor, $S(q)$,[7,8,9]

$$\varrho(r) = \varrho_0 + \frac{1}{2\pi^2 r}\int_0^Q dq\, q \sin(qr)\big[S(q)-1\big]\,, \qquad (1)$$

with atomic number density ϱ_0. For simplicity, we neglected multiphonon processes (*i.e.*, two-phonon and higher-order processes) in the computation of the diffuse scattering part of $S(q)$.[10] Thus, we assumed that the one-phonon scattering process is the dominant inelastic scattering process in the range of usually *measured* scattering vectors, $q < Q \sim 35 - 40\text{Å}^{-1}$. However, as was pointed out earlier,[2,11,12] one needs to be more careful about multiphonon contributions when comparing with actual experiments.

We fit the synthetic PDF data sets $\varrho_{\text{synth}}(r_i)$ with respect to the force constants of the model by minimizing the function

$$\chi^2_{\text{pdf}} = \frac{1}{N-F}\sum_{i=1}^{N}\frac{\big[\varrho_{\text{synth}}(r_i) - \varrho(r_i)\big]^2}{\sigma^2(r_i)}\,, \qquad (2)$$

where F is the number of force constants being fitted, and $N \gg F$. The number of spatial points is of the

order of $N \sim 1000$, and $\sigma(r_i) = \varepsilon_\sigma \varrho(r_*) r_*/r_i$ is an error estimate for $\varrho_{\rm synth}(r_i)$.[9] We use a relative error $\varepsilon_\sigma \approx 0.03$ at the first PDF peak maximum at distance r_*, which is typical for experiments with good neutron counting statistics and proper background corrections. Values as low as $\varepsilon_\sigma \approx 0.01$ are feasible in high-precision diffraction experiments. Since ε_σ enters in Eq. 2 only as an overall scaling factor, none of our results depend on the absolute value of ε_σ. The sums run from just below the first peak through $r_N = 1$nm. Extending the sum to $r_N = 2$nm does not lead to any significant changes in our results. The model PDF $\varrho(r_i)$ depends implicitly on the phonon dispersion and, thus, on the fitted force constants.

One starts the loop of the fitting procedure with a (small) set of plausible force constants and calculates the phonon frequencies $f(\mathbf{k}s)$ and eigenvectors $\mathbf{e}(\mathbf{k}s)$ on a fine mesh in the BZ. The computation of the static structure factor in the one-phonon approximation is straightforward, once the frequencies and eigenvectors are known. Finally, one computes the model PDF by convoluting the static structure factor with the instrumental resolution function of the diffractometer[13] and compares it with the synthetic PDF. An update of the force constants follows. These steps are repeated until a termination criterion is met, either in the implemented reverse Monte Carlo or Levenberg-Marquardt method. Since the Monte Carlo method is computationally intensive and slow compared to a generalized nonlinear least-squares minimizer, we tested the reverse Monte Carlo method only for models with a small set of fitting parameters.

Next we checked the quality of the resulting phonon dispersions by comparing the second phonon moment f_2 and the phonon dispersion $f(\mathbf{k}s)$ with the synthetic phonon data. The second moment of a monatomic crystal is defined by[6]

$$f_2 = \left(\frac{5}{9 N_{\rm BZ}} \sum_{s=1}^{3} \sum_{\mathbf{k} \in {\rm BZ}} f^2(\mathbf{k}s) \right)^{1/2}, \qquad (3)$$

with wave vector $\mathbf{k}$, phonon branch index s, and $N_{\rm BZ}$ $\mathbf{k}$-points in the summation over the Brillouin zone.

In order to quantify the goodness of the phonon dispersion we introduce the merit function

$$\chi^2_{\rm phon} = \frac{1}{N_p - F} \sum_{i=1}^{N_p} \frac{\left[f_{\rm synth}(\mathbf{k}_i s_i) - f(\mathbf{k}_i s_i) \right]^2}{\sigma_p^2(\mathbf{k}_i s_i)}, \qquad (4)$$

where N_p is the number of phonon frequencies. Their estimated errors σ_p are taken to be two percent of the frequency, but at least 0.04THz. These are typical error estimates reported for neutron triple-axis spectroscopy experiments.

III. RESULTS

We studied in detail elemental Ni, Ag, Al, Ce and Pb (*fcc*), as well as Fe and Nb (*bcc*). Since we obtained very similar results for Ni and Ag, we will not discuss Ag separately. The results for *bcc* structures show very similar behavior to the ones with *fcc* structure. Ni has a simple phonon dispersion typical of monatomic *fcc* crystals that can be described very well by including only the first few nearest-neighbor (NN) shells of interatomic force constants in a BvK model. On the other hand, Pb shows a complex dispersion (even when neglecting Kohn anomalies) that requires long-range forces up through 8NN shells in a BvK model. Similarly, Fe is the prototype of a monatomic *bcc* crystal with a simple phonon dispersion, whereas Nb possesses a very complex dispersion.

For each material we used two very different sets of initial force constants (set #1 and set #2) to start the fit procedure, in order to test the robustness of the minimization methods. In the *fcc* simulations shown in Figs. 1 through 8, we initialized the first shell (1NN) of force constants only (i.e., 3 parameters), either by using the correct elastic constants (set #1), or by the corresponding values of the 1NN force constants of the synthetic model (set #2). Note that in cubic systems the three independent elastic constants are uniquely defined by three force constants (see Appendix). In the case of the *bcc* structures we initialized the combined four force constants of the 1NN and 2NN shells (with the 2NN force constant $XY_2 \equiv 0$), either by using the correct elastic constants (set #1), or by the corresponding values of the synthetic model (set #2),

Also, for large numbers of force constants the Levenberg-Marquardt algorithm does not always converge to the global minimum. Instead it gets easily trapped in local minima, depending on the initial values of the force constants. If the initial values are chosen poorly, then this failure is almost unavoidable.

In the following subsections A through E we address in detail the quality and difficulties of fitting the PDF curves and investigate the quality of the corresponding phonon dispersion curves, phonon moments, elastic constants, Debye-Waller factors, and PDF peakwidths for a large set of elemental materials. We show results for systems that range progressively from very simple to very complex phonon models by gradually increasing the number of nearest-neighbor interatomic forces in a Born-von Kármán model. In figures 1 through 12 we present a comprehensive study of the inverse problem of extracting phonons from PDF curves from elemental cubic materials.

A. Goodness of Fit

It is obvious from our results for Ni, Al, Ce and Pb displayed in Figs. 1 through 8, and for Fe and Nb in Figs. 9 through 12, that the PDF is rather insensitive to the zone boundary phonons. This is best seen for the cases of Al, Ce, Pb and Nb, which have complex phonon dispersions with anomalies close to the Brillouin zone boundaries. In

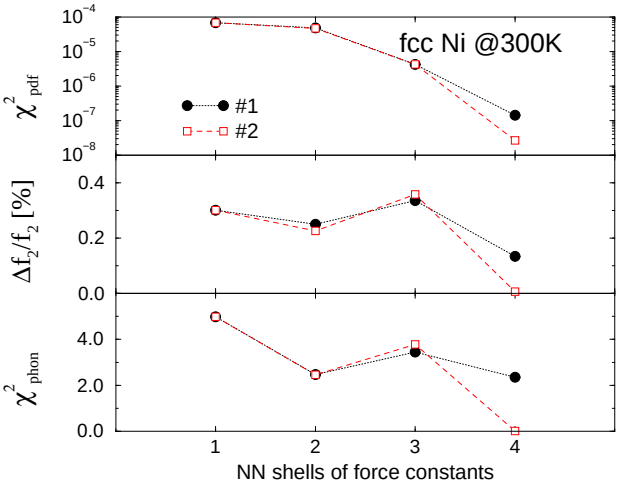


FIG. 1: Fitting the synthetic PDF of Ni, generated with a 4NN BvK force model. Top: PDF fits vs. number of nearest-neighbor shells of force constants for two different sets (#1 and #2). Center: Relative error of f_2 in percent of $f_2^{\rm synth} = 8.03$THz. Bottom: Figure of merit of computed phonon dispersions shown in Fig. 2

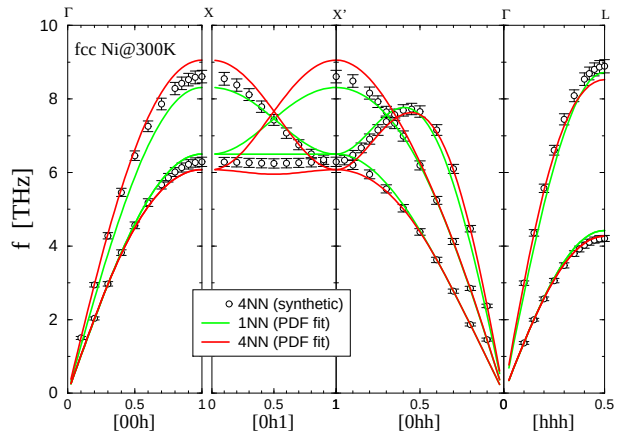


FIG. 2: (color) Phonon dispersions along high symmetry directions of the Brillouin zone obtained from fitting the PDF curve of a generalized 4NN BvK force model,[6] using fit models with 1NN and up to 4NN shells (set #1).

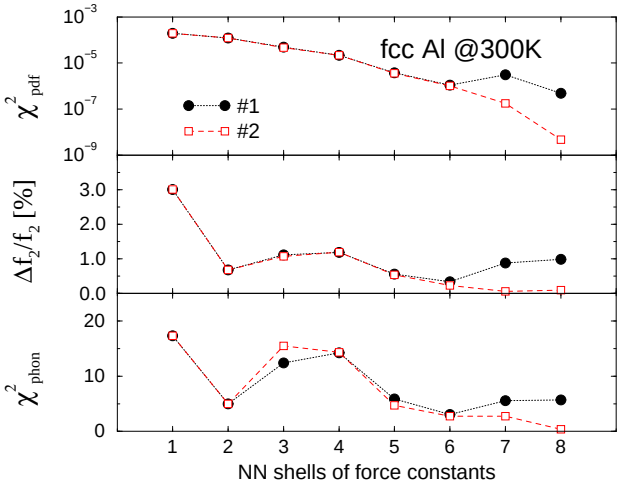


FIG. 3: Fitting the synthetic PDF of Al, generated with an 8NN BvK force model. Top: PDF fits vs. number of nearest-neighbor shells of force constants for two different sets (#1 and #2). Center: Relative error of f_2 in percent of $f_2^{\rm synth} = 8.28$THz. Bottom: Figure of merit of computed phonon dispersions shown in Fig. 4

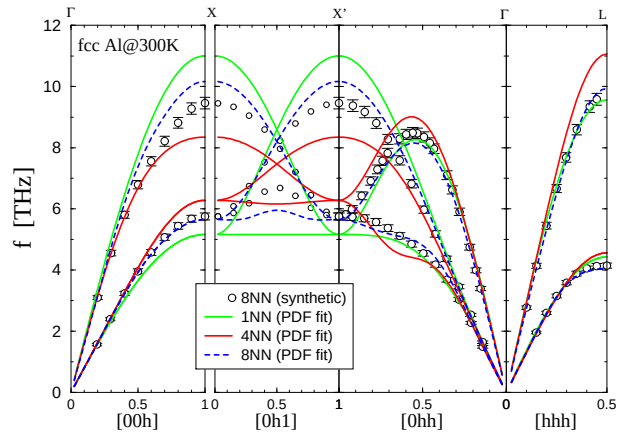


FIG. 4: (color) Phonon dispersions obtained from fitting the PDF curve of a generalized 8NN BvK force model,[6] using fit models with 1NN and up to 4NN and 8NN shells (set #1). Only frequencies (circles) with error bars are included in the computation of $\chi^2_{\rm phon}$ in Fig. 3.

other words, the PDF is not sensitive enough to register the out-of-phase motions of neighboring atoms.

Also there is no direct correlation between the goodness of the PDF fit $\chi^2_{\rm pdf}$ and the merit function of the phonon dispersion $\chi^2_{\rm phon}$. For example, in Fig. 7 it can be seen for the metal Pb that $\chi^2_{\rm pdf}$ of set #1 is an order of magnitude smaller than $\chi^2_{\rm pdf}$ of set #2 for 4NN and 5NN BvK models. However, their corresponding $\chi^2_{\rm phon}$ are reversed. This means that a good PDF fit can result in a bad description of the phonon dispersion, and vice versa. Similar conclusions follow from our study of Nb in Fig. 11. This is a very important finding. Hence it is generally not possible to provide a useful mapping between PDF spectra and phonon dispersion curves to solve the inverse problem. We find that $\chi^2_{\rm pdf}$ and $\chi^2_{\rm phon}$ are correlated overall only for simple metals (Ni, Ag and Fe) and semi-complex metals (Al and Ce), and that both fits improve asymptotically by adding more force constants to the phonon models. This demonstrates that our algorithm successfully solves the inverse problem for simple

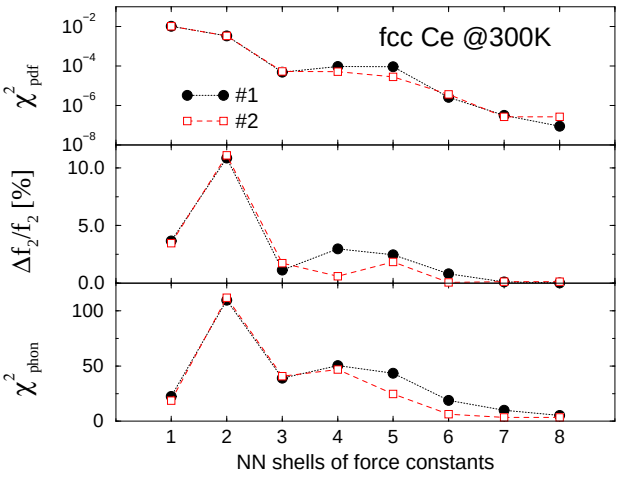


FIG. 5: Fitting the synthetic PDF of Ce, generated with an 8NN BvK force model. Top: PDF fits vs. number of nearest-neighbor shells of force constants for two different sets (#1 and #2). Center: Relative error of f_2 in percent of $f_2^{\rm synth} = 2.48$THz. Bottom: Figure of merit of computed phonon dispersions shown in Fig. 6

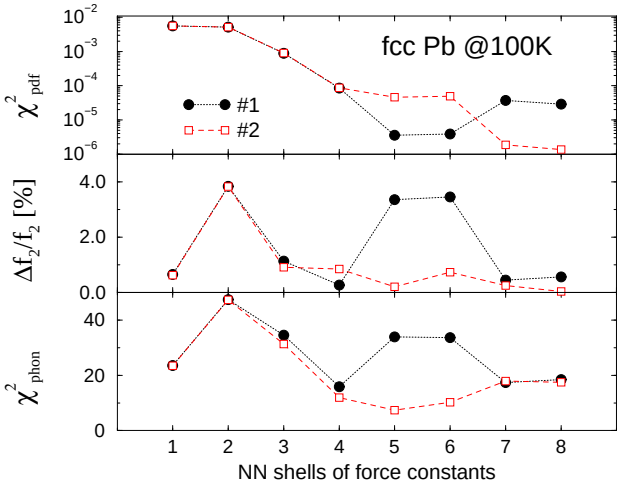


FIG. 7: Fitting the synthetic PDF of Pb, generated with an 8NN BvK force model. Top: PDF fits vs. number of nearest-neighbor shells of force constants for two different sets (#1 and #2). Center: Relative error of f_2 in percent of $f_2^{\rm synth} = 1.99$THz. Bottom: Figure of merit of the computed phonon dispersions shown in Fig. 8

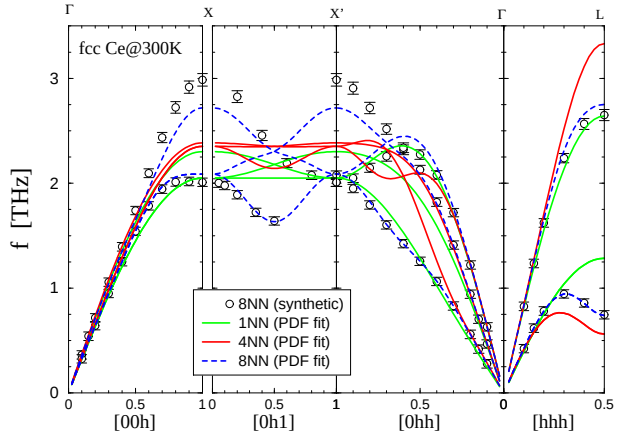


FIG. 6: (color) Phonon dispersions obtained from fitting the PDF curve of a generalized 8NN BvK force model,[6] using fit models with 1NN and up to 4NN and 8NN shells (set #1).

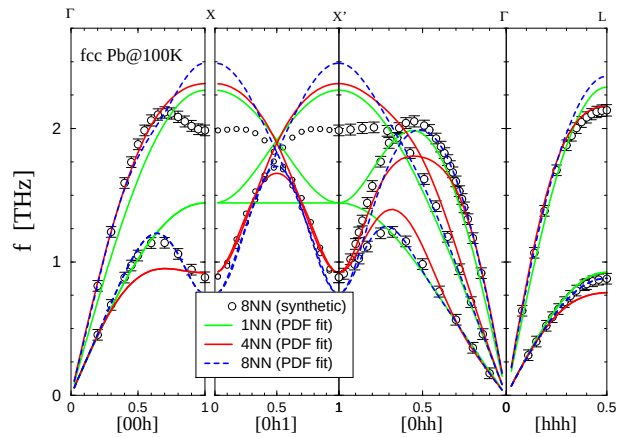


FIG. 8: (color) Phonon dispersions obtained from fitting the PDF curve of a generalized 8NN BvK model,[14] using fit models with 1NN, and up to 4NN and 8NN shells of force constants (set #1). Only frequencies (circles) with error bars are included in the computation of $\chi^2_{\rm phon}$ in Fig. 7.

cases if the PDF spectra can be obtained with arbitrarily high accuracy. At this point it is not clear if this is a robust result that will survive once actual experimental data sets are studied (by including statistical and systematic errors into the computation of $S(q)$). Thus, it is generally not possible to quantify *a priori* the quality of the extracted phonon dispersions based on $\chi^2_{\rm pdf}$.

All PDF fits to the synthetic data sets are almost indistinguishable, as follows from the extremely small values of $\chi^2_{\rm pdf}$ (see figures). This means that even the crudest BvK phonon model with only 1NN interatomic forces deviates on average less than $0.1 - 1\%$ from the synthetic PDF data, which is in good agreement with the analysis of the *forward* problem in Ref. 2. In any realistic experiment, where statistical and systematic measurement errors may result in a $\chi^2_{\rm pdf}$ of order one, it will be nearly impossible to attribute a tiny reduction of less than 10^{-3} in $\chi^2_{\rm pdf}$ to a significantly improved fit. Hence, in a realistic simulation a PDF fit with a simple 1NN BvK phonon model will be almost indistinguishable from one with a more complex 4NN or 8NN BvK model.

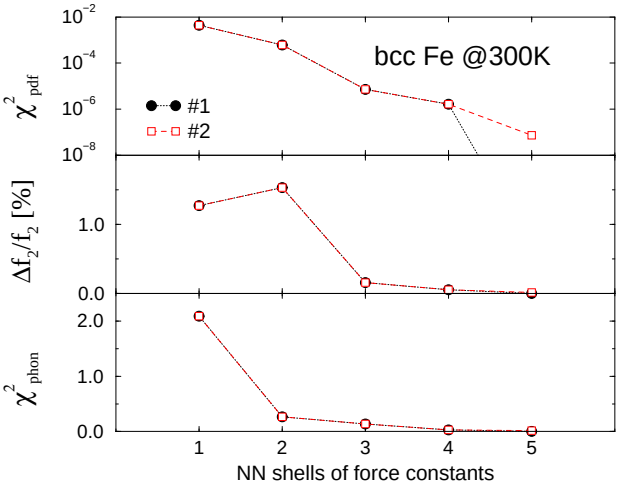


FIG. 9: Fitting the synthetic PDF of Fe, generated with a 5NN BvK force model. Top: PDF fits vs. number of nearest-neighbor shells of force constants for two different sets (#1 and #2). Center: Relative error of f_2 in percent of $f_2^{\rm synth} = 8.77$THz. Bottom: Figure of merit of computed phonon dispersions shown in Fig. 10

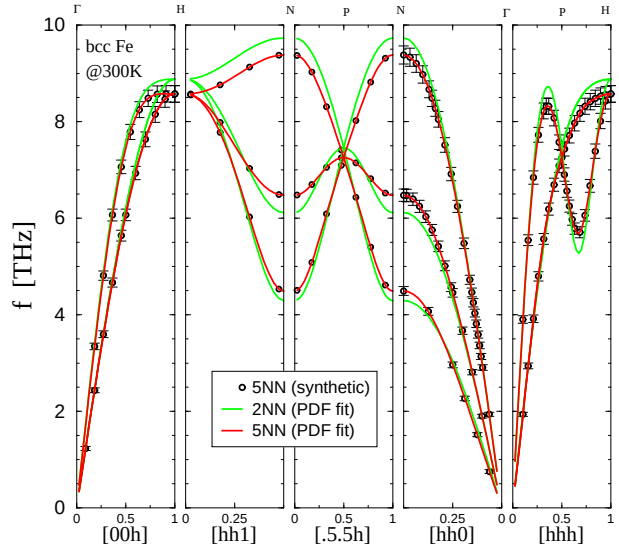


FIG. 10: (color) Phonon dispersions obtained from fitting the PDF of a generalized 5NN BvK force model,[6] using fit models with up to 2NN and 5NN shells (set #1). Only frequencies (circles) with error bars are included in the computation of $\chi^2_{\rm phon}$ in Fig. 9.

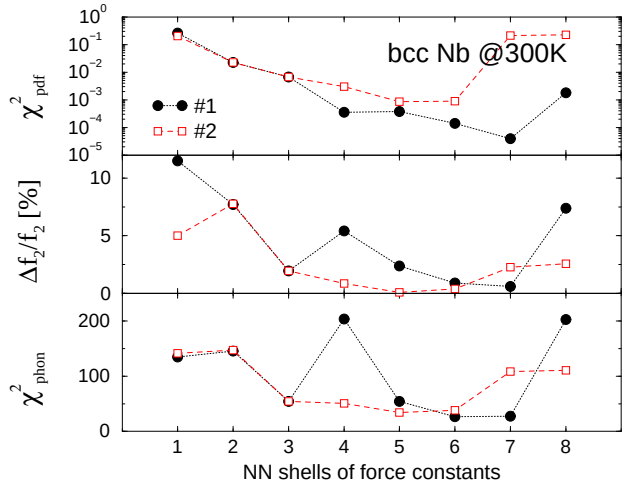


FIG. 11: Fitting the synthetic PDF of Nb, generated with an 8NN BvK force model. Top: PDF fits vs. number of nearest-neighbor shells of force constants for two different sets (#1 and #2). Center: Relative error of f_2 in percent of $f_2^{\rm synth} = 5.86$THz. Bottom: Figure of merit of computed phonon dispersions shown in Fig. 12

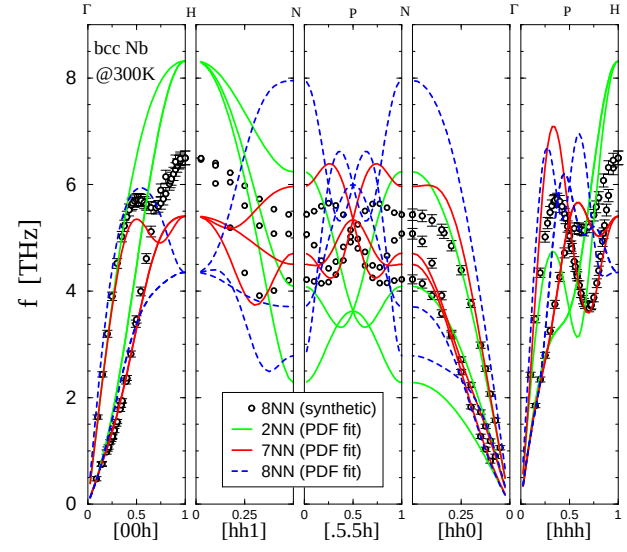


FIG. 12: (color) Phonon dispersions obtained from fitting the PDF of a generalized 8NN BvK force model,[6] using fit models with up to 2NN, 7NN and 8NN shells (set #1). Only frequencies (circles) with error bars are included in the computation of $\chi^2_{\rm phon}$ in Fig. 11.

B. Phonon Moments

Since phonon moments are an integrated quantity of the phonon dispersion curves, it is plausible to expect them to be less sensitive to the details of the phonon models being used to generate them. This is indeed the case, as can be seen for the second moment shown in figures 1, 3, 5, 7, 9, and 11. Here we focus on the second moment only, because (1) it is more sensitive to high frequencies (near the zone boundaries) than the lower moments, and (2) it enters the free energy functional in the high-temperature limit, and can be obtained inde-

pendently in a specific heat measurement. For simple and semi-complex dispersion curves (Ni, Ag, Fe, and Al, Ce) the relative errors of the computed second phonon moments track the overall goodness of the PDF fit. Unfortunately, this is not true for more complex dispersions (Pb and Nb), where we could not establish a correlation between the goodness of $\chi^2_{\rm pdf}$ and the relative error of the second moment $\Delta f_2/f_2^{\rm synth} = |f_2 - f_2^{\rm synth}|/f_2^{\rm synth}$. However, even systems with complex phonon dispersions allow the extraction of phonon moments within a few percent of accuracy. Several years ago Knapp *et al.*[15] arrived at similar conclusions while studying the mean-square relative displacement of the central atom in *fcc* materials with extended x-ray absorption fine-structure measurements.

Finally, our computations for Ce, Pb, and Nb show that the second phonon moment is too insensitive to the phonons at the zone boundaries of the Brillouin zone to be useful for determining zone boundary phonons.

C. Elastic Constants

Dimitrov and co-workers[1] suggested that by adding *measured* elastic constants as constraints to the PDF fit (constrained fit) one can improve upon the extracted phonon dispersions. This is contrary to our own results. We could not observe any significant changes to our extracted phonon dispersions by using constrained PDF fits; *i.e.*, constraining the PDF fit to give force constants that yield the correct elastic constants does not result in better phonon dispersions near the zone boundaries. Of course it results in slightly more accurate phonon dispersions near the zone center. This is not surprising since the elastic constants determine the long-wavelength limit of the phonon dispersions at the center of the Brillouin zone (Γ point) and not at the zone boundaries, where the discrepancies between the *synthetic* phonon dispersions and the PDF-fitted phonon dispersions are largest. Here the extracted phonon dispersions could improve by providing additional constraints on zone boundary phonons.

Furthermore, our analysis shows that, in many cases, the unconstrained PDF fits already yield elastic constants that deviate only a few percent (approximately $1-6\%$) from the values of the elastic constants of the *synthetic* data sets, when a significantly large number of force constants are being used. By "sufficiently large", we mean at least a 3NN BvK force model for Ni, Ag, Ce and Fe and a 5NN BvK model for Al and Pb. This does not work for Nb, however, where the extracted elastic constants are more than 10% off, even for the best fit. For a definition of the elastic constants in terms of a BvK force model for *fcc* and *bcc* crystal structures see the Appendix.

D. Debye-Waller Factor

Reichardt and Pintschovius suggested that it might be possible to improve the quality of extracted phonon dispersions by adding constraints to the PDF fit, *e.g.*, thermal parameters independently measured by a Rietveld analysis. The thermal parameters, which are given by the exponent of the Debye-Waller factor, e^{-2W}, measure the mean-square atomic displacement $\langle u^2\rangle$. For cubic crystals the Debye-Waller exponent simplifies to[7]

$$2W(\mathbf{q}) \;=\; \langle(\mathbf{q}\cdot\mathbf{u})^2\rangle = q^2\langle u^2_{\mathbf{q}}\rangle = \frac{1}{3}q^2\langle u^2\rangle\,, \qquad (5)$$

where $u_{\mathbf{q}}$ is the component of the displacement vector $\mathbf{u}$ in the direction of the scattering vector $\mathbf{q}$. This result may be expressed another way,

$$\begin{aligned} W(\mathbf{q}) \;&=\; \frac{\hbar}{4MN_{\rm BZ}}\sum_s\sum_{\mathbf{k}\in{\rm BZ}}\frac{\left|\mathbf{q}\cdot\mathbf{e}(\mathbf{k}s)\right|^2}{\omega(\mathbf{k}s)}\coth\left(\frac{\hbar\omega(\mathbf{k}s)}{2k_BT}\right) \\ &=\; \frac{\hbar q^2}{4M}\int_0^\infty d\omega\;\mathcal{W}(\omega)\,, \end{aligned} \qquad (6)$$

with the Debye-Waller spectral function given by

$$\mathcal{W}(\omega) = \frac{N(\omega)}{\omega}\coth\left(\frac{\hbar\omega}{2k_BT}\right)\,, \qquad (7)$$

where M is the atomic mass, $\omega(\mathbf{k}s)$ is the angular frequency of mode s, and $\mathbf{e}(\mathbf{k}s)$ is its normalized eigenvector. The phonon density of states is normalized so that

$$\int_0^\infty d\omega N(\omega) = 1\,, \qquad (8)$$

and $N(\omega)\equiv 0$ for ω larger than the maximum phonon frequency. The thermal parameters extracted from our PDF fits are remarkably insensitive to the specific form of the phonon model. Even for the simplest phonon models used, the relative error of $\langle u^2\rangle$ is typically less than 1% (less than 0.1% for Ni, Ag, Al, and Pb) and less than 5% for Nb. Thus, measured thermal parameters, whose absolute values are known only within 5%, cannot give improved PDF fits or better phonon dispersions.

At this point a caveat is needed for using elastic constants (derived from long wavelength modes) and a Debye phonon model to estimate the Debye-Waller factor, or when comparing Debye temperatures with Debye-Waller factors measured at high temperatures. Figs. 13 and 14 show very clearly for Ni and Ce that at room temperature the Debye-Waller spectral function $\mathcal{W}(\omega)$ estimated from the long wavelength modes, is only a crude approximation. It consistently underestimates the contribution of the intermediate frequency region (transverse modes near the zone boundary), and describes the high frequency region (longitudinal modes near the zone boundary) only on average. Here the Debye-Waller exponents $2W$ computed from a Debye phonon model are 20% too small,

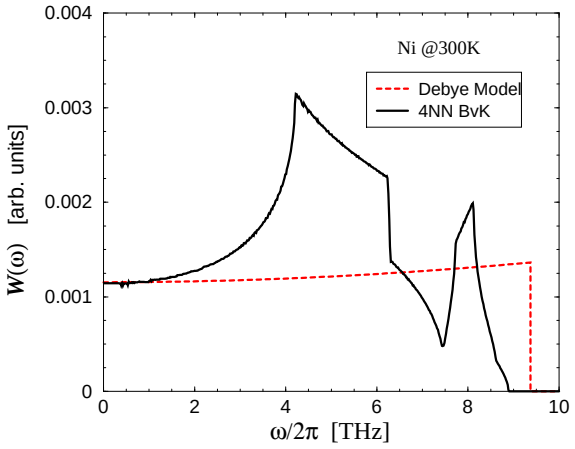


FIG. 13: A comparison of the Debye-Waller spectral functions of Ni at 300K for a realistic 4NN BvK phonon model[6] with its corresponding Debye phonon model.

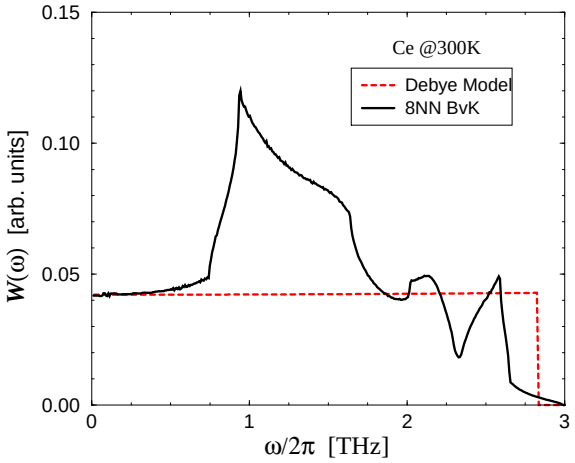


FIG. 14: A comparison of the Debye-Waller spectral functions of Ce at 300K for a realistic 8NN BvK phonon model[6] with its corresponding Debye phonon model.

compared to the ones using more realistic lattice dynamical models. The other materials studied show similar discrepancies, except in the case of Nb where both the Debye and lattice model calculations of the thermal parameters accidentally agree within 1 percent. Indeed, it is well known that the Debye-Waller factor is rather insensitive to the detailed form of the phonon dispersion, and at high temperatures it depends only on a single parameter, namely, the inverse-squared phonon moment.[16]

E. PDF Peakwidths

For studying local atomic structure properties in semiconductors Chung and Thorpe[11] used a real space approach to compute the PDF. They showed in the harmonic approximation that the PDF is approximately a series of Gaussian peaks, each centered at distance r_i with width σ_i,

$$\sigma_i^2 = \frac{\hbar}{MN_{\rm BZ}} \sum_s \sum_{\mathbf{k}\in {\rm BZ}} \coth\left(\frac{\hbar\omega(\mathbf{k}s)}{2k_BT}\right) \frac{|\hat{r}_i\cdot\mathbf{e}(\mathbf{k}s)|^2}{\omega(\mathbf{k}s)} \times\left[1-\cos(\mathbf{k}\cdot\mathbf{r}_i)\right]. \quad (9)$$

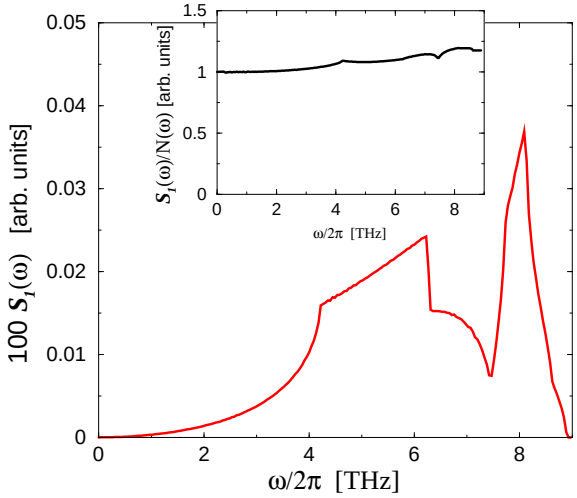


FIG. 15: The spectral function of the first PDF peak of Ni at 300K. Insert: $\mathcal{S}_1(\omega)/N(\omega)$ is nearly constant for frequencies $\omega < \omega_{\rm max}/2$. This frequency range is significantly smaller for Pb and Nb and marks the deviation from a Debye-model phonon spectrum.

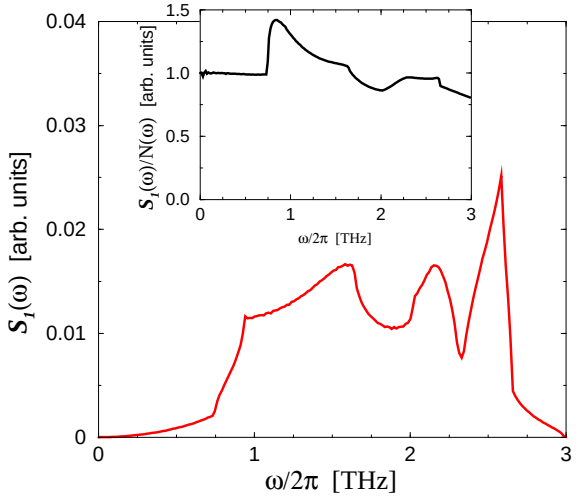


FIG. 16: The spectral function of the first PDF peak of Ce at 300K. Insert: $\mathcal{S}_1(\omega)/N(\omega)$ is nearly constant for frequencies $\omega < \omega_{\rm max}/4$.

Here $\mathbf{r}_i$ is a position vector of an atom in the i-th NN shell measured relative to an atom at the origin, and $\hat{r}_i = \mathbf{r}_i/r_i$. In the limit $\mathbf{k}\cdot\mathbf{r}_i \gg 1$ the cosine term oscillates so rapidly across the BZ that its average vanishes and the peakwidths of far-out atoms contain the same information as the Debye-Waller exponent, namely, $\lim_{i\to\infty}\sigma_i^2 \equiv \sigma_\infty^2 = 4W(q)/q^2$. This explains why the PDF fits reproduce the Debye-Waller factors so well, and that adding thermal parameters cannot provide any extra constraints.

On the other hand, the width of the first PDF peak (which is the sum of the auto-correlation and cross-correlation parts of the displacement-displacement function) exhibits the largest deviations from the long-range value σ_∞^2 (which is purely the auto-correlation part of the displacement-displacement function), due to the short-range nature of correlations of lattice vibrations. Note that in the real space approach all multiphonon processes have been included. Expanding $\cos(\mathbf{k}\cdot\mathbf{r}_i)$ in Eq. 9, it follows that at high temperatures and for low frequencies the spectral function of σ_i^2 is, in first-order approximation, dominated by the phonon density of states. We define the spectral function $\mathcal{S}_i(\omega)$ of the i-th peak as

$$\sigma_i^2 = \frac{\hbar}{M}\int_0^\infty d\omega\ \mathcal{S}_i(\omega)\,, \tag{10}$$

$$\mathcal{S}_i(\omega) = \mathcal{W}(\omega)\left\langle|\hat{r}_i\cdot\mathbf{e}(\mathbf{k}s)|^2[1-\cos(\mathbf{k}\cdot\mathbf{r}_i)]\right\rangle_\omega, \tag{11}$$

where $\langle\ldots\rangle_\omega$ is a normalized average over phonon modes and $\mathbf{k}$-points at fixed frequency, $\omega(\mathbf{k}s)=\omega$, and $\mathcal{S}_i(\omega)\equiv 0$ for frequencies larger than the maximum phonon frequency. For sufficiently small frequencies we get $\left\langle|\hat{r}_1\cdot\mathbf{e}(\mathbf{k}s)|^2[1-\cos(\mathbf{k}\cdot\mathbf{r}_1)]\right\rangle_\omega \sim k^2a^2 \sim (a/c)^2\omega^2$, with the average sound speed c and lattice constant a. For temperatures $T \gg \hbar\omega/2k_B$, the width of the first peak is a rough measure of the integrated phonon density of states times $\frac{\hbar}{M}\frac{a^2}{c^2}$, as can be seen in the inserts of Figs. 15 and 16.

It is not too surprising to find that the widths of the first peak and that of very distant peaks, or equivalently the Debye-Waller factor, are crudely approximated by long wavelength phonons, although for quite different physical reasons. Since for purely elastic neutron scattering the peakwidths are identical, $\sigma_i^2 = \sigma_\infty^2 = 4W(q)/q^2$,[16] and in most metals inelastic scattering (one-phonon, two-phonon, and higher-order processes) leads only to small corrections $\triangle\sigma_1$ of order $10-30\%$ in the width of the first peak σ_1, one does not expect large variations in σ_i. Hence the magnitude of the peakwidths will be approximated in leading order by the long wavelength phonons. For example, in the case of Ni we find a difference of $\triangle\sigma_1/\sigma_1 \approx 13\%$ between the fitted PDF curve that includes only elastic processes versus elastic plus one-phonon processes. For Al and Pb we obtain $\triangle\sigma_1/\sigma_1 \approx 25\%$. These one-phonon corrections are largest for the first PDF peak and much smaller for the other peaks.[2,12]

IV. CONCLUSIONS

In conclusion, our study shows that one cannot obtain accurate phonon dispersions from an inverse analysis of the pair-density function, unless the lattice dynamics are simple and fully described by a few phonon parameters, as in the cases of *fcc* Ni and Ag and *bcc* Fe, for example. A semi-quantitative picture of the phonon dispersion may be obtained in simple and semi-complex metals, but not in metals with complex phonon dispersions. In principle, in simple metals phonon frequencies can be extracted within a few percent accuracy ($\sim 2-8\%$) in the entire Brillouin zone, whereas in semi-complex and complex metals such accuracy applies only to a small fraction of the Brillouin zone centered around the Γ-point with wave vector $k \lesssim \pi/4a$. We found numerically that the pair-density function provides an overall account of the lattice dynamics by yielding phonon moments within a few percent accuracy. In other words, a rather simple phonon model suffices to describe the dynamics embedded in powder diffraction data. Neutron or x-ray PDF studies play an important role in the studies of the local structure of crystals, but cannot provide deeper insight into the dynamics of lattice vibrations. A more promising approach for extracting phonons from powders or polycrystals may be the analysis of time-of-flight spectra from inelastic neutron scattering.[17,18]

Acknowledgments

We thank D. Wallace, A. Lawson, H. Röder, L. Pintschovius, D. Strauch and G. Eckold for many helpful discussions and especially J. Wills for helping with the symmetry operations and $\mathbf{k}$-point summations. This work was supported by the Los Alamos National Laboratory under the auspices of the U.S. Department of Energy.

APPENDIX: ELASTIC CONSTANTS IN A BORN-VON KÁRMÁN FORCE MODEL

In a cubic crystal there are only three independent elastic constants.[19] For *fcc* crystal structures with lattice constant a these are related to the force constants (up through 8NN interatomic shells) by

$$\begin{aligned} aC_{11} = {} & 4XX_1 + 4XX_2 + 16XX_3 + 8YY_3 + 16XX_4 + \\ & 36XX_5 + 4YY_5 + 16XX_6 + 72XX_7 + \\ & 32YY_7 + 8ZZ_7 + 16XX_8\,, \end{aligned} \tag{A.1}$$

$$\begin{aligned} aC_{44} = {} & 2XX_1 + 2ZZ_1 + 4YY_2 + 4XX_3 + 20YY_3 + \\ & 8XX_4 + 8ZZ_4 + 2XX_5 + 18YY_5 + 20ZZ_5 + \\ & 16XX_6 + 20XX_7 + +40YY_7 + \\ & 52ZZ_7 + 16YY_8\,, \end{aligned} \tag{A.2}$$

$$a(C_{12}+C_{44}) = 4XY_1 + 8YZ_3 + 32XZ_3 + 16XY_4 + 24XY_5 + 32YZ_6 + 96XY_7 + 48XZ_7 + 32YZ_7\,, \quad \text{(A.3)}$$

and for *bcc* structures these are given by

$$aC_{11} = 2XX_1 + 2XX_2 + 8XX_3 + 18XX_4 + 4YY_4 + 8XX_5 + 8XX_6 + 36XX_7 + 2ZZ_7 + 32XX_8 + 8YY_8\,, \quad \text{(A.4)}$$

$$aC_{44} = 2XX_1 + 2YY_2 + 4XX_3 + 4ZZ_3 + 2XX_4 + 20YY_4 + 8XX_5 + 8YY_6 + 20XX_7 + 18ZZ_7 + 4XX_8 + 16YY_8 + 20ZZ_8\,, \quad \text{(A.5)}$$

$$a(C_{12}+C_{44}) = 4XY_1 + 8XY_3 + 4YZ_4 + 24XY_4 + 16XY_5 + 24YZ_7 + 36XY_7 + 32XY_8\,, \quad \text{(A.6)}$$

where we followed the derivation of Squires.[20,21] Our elastic constants agree with those in Ref. 20 where comparison is possible, except for the term $4YY_4$ in C_{11} for *bcc* structures. The generalized BvK force matrix of the n-th NN interatomic shell is defined by

$$\mathbf{\Phi}_{\mathrm{nNN}} = \begin{pmatrix} XX_n & XY_n & XZ_n \\ XY_n & YY_n & YZ_n \\ XZ_n & YZ_n & ZZ_n \end{pmatrix}. \quad \text{(A.7)}$$

Its symmetry properties are listed in Table I.

TABLE I: Symmetries of the generalized BvK force constant matrix $\mathbf{\Phi}_{\mathrm{nNN}}$ for monatomic *fcc* and *bcc* crystal structures. The lattice indexes $[h_1h_2h_3]$ refer to lattice positions $(h_1,h_2,h_3)a/2$ with $h_1 \geq h_2 \geq h_3$.

shell	fcc	bcc
1NN	[110]	[111]
	$XX_1 = YY_1$	$XX_1 = YY_1 = ZZ_1$
	$XZ_1 = YZ_1 = 0$	$XY_1 = XZ_1 = YZ_1$
2NN	[200]	[200]
	$YY_2 = ZZ_2$	$YY_2 = ZZ_2$
	$XY_2 = XZ_2 = YZ_2 = 0$	$XY_2 = XZ_2 = YZ_2 = 0$
3NN	[211]	[220]
	$YY_3 = ZZ_3$	$XX_3 = YY_3$
	$XY_3 = XZ_3$	$XZ_3 = YZ_3 = 0$
4NN	[220]	[311]
	$XX_4 = YY_4$	$YY_4 = ZZ_4$
	$XZ_4 = YZ_4 = 0$	$XY_4 = XZ_4$
5NN	[310]	[222]
	$XZ_5 = YZ_5 = 0$	$XX_5 = YY_5 = ZZ_5$
	–	$XY_5 = XZ_5 = YZ_5$
6NN	[222]	[400]
	$XX_6 = YY_6 = ZZ_6$	$YY_6 = ZZ_6$
	$XY_6 = XZ_6 = YZ_6$	$XY_6 = XZ_6 = YZ_6 = 0$
7NN	[321]	[331]
	–	$XX_7 = YY_7$, $XZ_7 = YZ_7$
8NN	[400]	[420]
	$YY_8 = ZZ_8$	$XZ_8 = YZ_8 = 0$
	$XY_8 = XZ_8 = YZ_8 = 0$	–

[1] D.A. Dimitrov, D. Louca, and H. Röder, Phys. Rev. B **60**, 6204 (1999).

[2] W. Reichardt and L. Pintschovius, Phys. Rev. B **63**, 174302 (2001).

[3] A. Mellergård and R.L. McGreevy, Chem. Phys. **261**, 267 (2000).

[4] A. Corana, M. Marchesi, C. Martini, and S. Ridella, ACM Transactions Math. Software **13**, 262 (1987).

[5] W.H. Press, S.A. Teucholsky, W.T. Vetterling, and B.P. Flannery, *Numerical Recipes in C* (Cambridge University Press, Cambridge, 1999).

[6] Landolt-Börnstein, *Metalle: Phononenzustände und Fermiflächen*, Vol. 13, edited by P.H. Dederichs, H. Schober, D.J. Sellmyer (Springer, New York, 1981).

[7] G.L. Squires, *Introduction to the Theory of Thermal Neutron Scattering*, (Dover Pub., Mineola, New York, 1996).

[8] S.L. Lovesey, *Theory of Neutron Scattering from Condensed Matter: Nuclear Scattering*, (Clarendon Press, Oxford, 1987)

[9] B.H. Toby and T. Egami, Acta Cryst. A - Fund. of Cryst. **48**, 336 (1992).

[10] We mimick the effects of multiphonon processes by adding a smooth function, $S_m(q) = 1 - \exp(-2W(q)/2.4)$, to the computation of the coherent static structure factor $S(q) = S_0(q) + S_1(q) + S_m(q)$. In addition to the elastic (S_0) and 1-phonon (S_1) coherent scattering contributions, S_m guarantees the correct asymptotic limits of $S(q)$, namely, $\lim_{q\to\infty} S(q) = 1$ and $\lim_{q\to 0} S(q) = 0$.

[11] J.S. Chung and M.F. Thorpe, Phys. Rev. B **55**, 1545 (1997).

[12] M.F. Thorpe, V. Levashov, M. Lei, and S.J.L. Billinge, *Notes on the analysis of data for pair distribution functions* in the proceedings of the workshop "From Semiconductors to Proteins: Beyond the Average Structure", July 28 - August 1, 2001, in Traverse City, Michigan, edited by S.J.L. Billinge and M.F. Thorpe, (Kluwer Academic/Plenum Publishers, New York, 2001), p. 105.

[13] We used a standard (non-gaussian) diffractometer resolution function (type I) as specified in the GSAS manual: A.C. Larson and R.B. von Dreele, *GSAS*, Los Alamos National Laboratory, Technical Report: LA-UR:86-748 (1986) [ftp://ftp.lanl.gov/public/gsas/manual].

[14] We used a slightly improved set of force constants for Pb that results in more accurate phonon frequencies near the zone boundaries than the one in Ref. 6.

[15] G.S. Knapp, H.K. Pan, and J.M. Tranquada, Phys. Rev. B **32**, 2006 (1985).

[16] W. Marshall and S.L. Lovesey, *Theory of Thermal Neutron Scattering*, (Clarendon Press, Oxford, 1971), p. 73.

[17] U. Buchenau *et al.*, Phys. Rev. B **27**, 955 (1983).

[18] M. Heiroth, U. Buchenau, H.R. Schober, and J. Evers, Phys. Rev. B **34**, 6681 (1986).

[19] D.C. Wallace, *Thermodynamics of Crystals*, (Dover Pub., Mineola, New York, 1998), Chap. 2.

[20] G.L. Squires, *The relation between the interatomic forces and the frequencies of symmetry phonons in cubic crystals* in the proceedings of the symposium on "Inelastic Scattering of Neutrons in Solids and Liquids", (IAEA Vienna, 1963), Vol. II, p. 71.
[21] G.L. Squires, Arkiv f. Fysik **25**, 21 (1962).